

## The search for crystal undulator radiation

**D Boshoff<sup>1</sup>, M Copeland<sup>1</sup>, F Haffejee<sup>1</sup>, Q Kilbourn<sup>1</sup>, B MacKenzie<sup>1</sup>, C Mercer<sup>1</sup>, A Osato<sup>1</sup>, C Williamson<sup>1</sup>, P Sihoyiya<sup>2</sup>, M Motsoai<sup>2</sup>, M Connell<sup>3</sup>, CA Henning<sup>1</sup>, SH Connell<sup>4</sup>, N L Palmer<sup>7</sup>, T Brooks<sup>5</sup>, J Härtwig<sup>4,6</sup>, TN Tran Thi<sup>6</sup>, U Uggerhøj<sup>8</sup> and the PEARL Collaboration<sup>8</sup>**

<sup>1</sup>St John's College, Houghton, South Africa, <sup>2</sup>Barnato Park High School, Berea, South Africa <sup>3</sup>King's College London, London, UK <sup>4</sup>University of Johannesburg, Auckland Park, South Africa <sup>5</sup>Royal Holloway College, University of London, UK <sup>6</sup>European Synchrotron Research Facility (ESRF), Grenoble, France <sup>7</sup>Element Six, Harwell, UK <sup>8</sup>Århus University, Århus, Denmark <sup>9</sup>The PEARL Collaboration of the European Commission project H2020-MSKA-RISE-2015

E-mail: shconnell@uj.ac.za

**Abstract.** The channelling phenomenon applies to the correlated motion of charged particles within a crystal lattice in a direction closely aligned with atomic rows (strings) or crystal planes. When the incident charge particle is highly relativistic, the emitted channeling radiation is boosted by a factor of  $\gamma^2$ , where  $\gamma$  is the Lorentz factor. Bremsstrahlung may also be coherent for these conditions, and coherent enhancement leads to both quasi monoenergetic peaks and also significant increases in intensity as compared to the normal process. In the special condition that the crystal is periodically bent, such as in a periodic superlattice, one may also have undulator radiation. All of these phenomena are potential sources of MeV and GeV range intense gamma radiation. The latter phenomenon is proposed as potentially the most important source of monochromatic high energy photons. In principle it can also lead to coherent radiation based on the Free Electron Laser (FEL) principle with intensities similar to an extrapolation of what may be obtained at modern light sources. In this contribution we describe a search for crystal undulator radiation using 2.5 – 6.0 GeV positrons incident on a diamond crystal undulator. The experiments were performed at the T9 Beam-line of the Proton Synchrotron at CERN. The experiment was the result of a winning proposal for the 2015 CERN Beam-line for Schools Competition.

### 1. Introduction

A crystal undulator is similar to a normal undulator [1] as typically found at a synchrotron for the production of extremely brilliant X-ray beams. The difference is that the magnetic lattice is realized by the periodic electrostatic potential of a crystal lattice as seen from the reference frame of an impinging GeV range electron or positron beam. The extremely relativistic incident particle beam has a crystallographically aligned incidence and is captured in a high index crystallographic channel of the crystal superlattice. The crystal lattice undulation period can be in the tens of microns scale. The particle beam will then “see” a many Tesla range periodically varying magnetic field. The larger fields and shorter undulator periods in the crystal undulator as compared to the conventional magnetic lattice undulator are significant. This method could theoretically lead to an MeV range gamma ray laser by the FEL principle.

This paper describes an attempt to commission a tagged photon beamline and then to measure undulator radiation (CUR) at the T9 beam-line of the CERN Proton Synchrotron (PS). The school based authors of this paper developed a successful proposal “Accelerating

Africa” to test a diamond crystal undulator within the CERN Beam-line for Schools [2] project. The goal of the experiment was to search for radiation enhancement effects related to aligned incidence of the positron beam on the diamond superlattice (undulator).

## 2. Parameters for the diamond crystal undulator

The theoretical feasibility study to produce powerful monochromatic undulator radiation in the gamma ray region by means of a crystal undulator (periodically bent crystal) and ultra relativistic light lepton beams (energy  $\epsilon_{e^+}$ ) impinging on the lattice with incidence aligned to a crystallographic axis is presented in several references [3, 4, 5] and references therein. Figure 1 indicates the trajectory of a charged particle captured in the channeling condition in a low index crystallographic direction. The channelled trajectory has an oscillation within the channel, leading to the emission of channeling radiation (CR, energy  $\epsilon_{ch}$ ). In addition the particle follows the periodic undulations of the lattice, and as such, it will also emit CUR (energy  $\epsilon_u$ ).

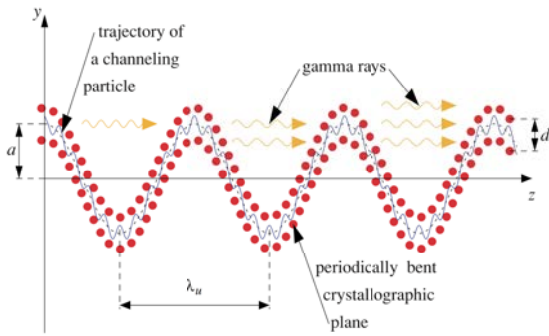


Figure 1: A charged particle captured in a undulating crystal channel [6].

The parameters for a Large Amplitude Long Period (LALP) diamond crystal undulator optimised for the positron beams available at the T9 beamline at the CERN PS are shown in Table 1, where an important condition is  $\lambda_u \gg a \gg d$ . These symbols are defined in Figure 1. This means  $\lambda_u > \lambda_c$  where  $\lambda_c$  is the CR wavelength, so that the CUR will have a lower energy than the CR. There is an alternative scenario known as Small Amplitude Short Period (SASP) where  $\lambda_u < \lambda_c$  and where  $a$  also has to be small [7]. Table 1 also collects the SASP parameters.

Table 1: Typical physical parameters for a 110 diamond crystal undulator for  $E_{e^+}$  few GeV.

Parameter	Value							
$\epsilon_{e^+}$ (GeV)	2	3	4	5	6	7	8	9
$L_{e^+}(0)$ ( $\mu\text{m}$ )	1059	1563	2061	2553	3042	3528	4012	4493
$L_{e^-}(0)$ ( $\mu\text{m}$ )	43	64	86	107	129	150	171	193
$\epsilon_{ch}$ (MeV)	9.6	17.6	27.0	37.8	49.7	62.6	76.5	91.3
$\epsilon_u$ (MeV) for SASP $\lambda_u = 600$ nm	60	140	240	370	0.52	700	900	1120
$\epsilon_u$ (MeV) for LALP $\lambda_u = 10$ $\mu\text{m}$	2			10				30

For the SASP case, the CUR is of a higher energy than the CR (one source of background). The brehmsstrahlung radiation (BR) has a  $1/E_\gamma$  photon energy distribution, which dominates for lower photon energies, so this is the principal source of background, especially for the LALP CUR case. Furthermore, in the SASP case, the undulator layers may be thinner, and therefore, currently, technologically more easily produced. A further effect to consider is the straight crystal dechanneling length  $L(0)$ , which is much larger for positrons than electrons, but where the overall length should still be minimised. For these reasons, a decision was made to first produce a SASP diamond crystal undulator for positron incidence in the proof of principle experiment.

## 3. The diamond graded superlattice

Doping diamond with single substitutional atoms of boron dilates the lattice. The boron can be introduced during the growth of synthetic diamond in the Chemical Vapour Deposition (CVD) process in a regulated way, leading to the periodic variation of the lattice constant.

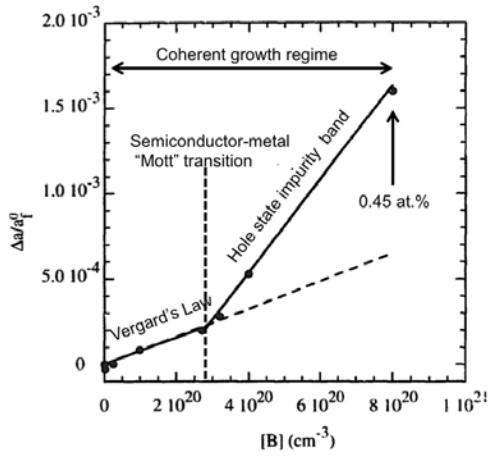


Figure 2: The lattice dilatation due to boron doping in diamond [8].

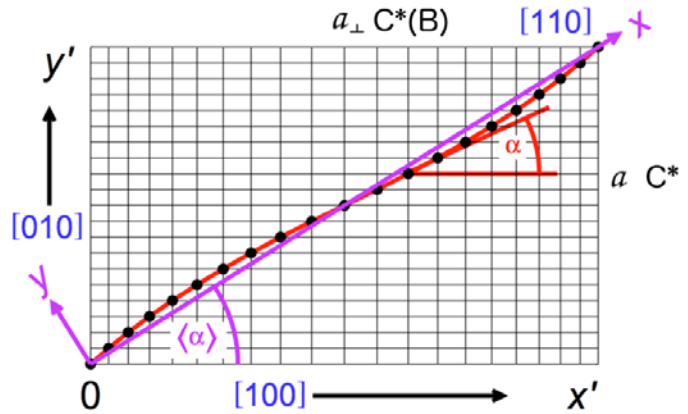


Figure 3: The development of an undulation in the 110 direction due to graded boron doping [9].

The measured lattice dilatation for diamond due to graded boron doping is taken from references [8, 10]. The boron is expected to be uniformly distributed in substitutional sites leading to epitaxial coherent layer growth following the diamond structure up to at least a boron concentration of  $C_B = 0.45\%$  (atomic). At first the dilatation effect proceeds based on Vergard's Law, and when the Mott transition is reached, the expansion is faster as the hole state impurity band modifies the Fermi level. Figure 2 quantifies this behaviour. The intrinsic substrate constrains the lattice to an expansion only in the growth direction, as shown in Figure 3. This longitudinal elongation is known as the Poisson effect and can be quantified using the elasticity constants for diamond together with the quantified dilatation behaviour, as well as a model for the progression of the undulator effect, as in the reference [9]. This leads to the determination of the undulation amplitude as a function of the boron doping concentration. This has been done in [9] but also in more detail with direct modelling in [11].

Element Six Technologies prepared a CVD grown diamond crystal undulator with the parameters  $\lambda_u \approx 0.6 \mu\text{m}$  and  $a \approx 0.4 \text{ \AA}$  with 6 such undulator layers on a  $300 \mu\text{m}$  High Pressure High Temperature (HPHT) synthetic diamond type Ib 110 oriented substrate. The diamond undulator was roughly pre-aligned using an on-line X-ray Laue system at the University of Johannesburg and then fine aligned using a highly collimated Bragg condition X-ray Diffraction.

#### 4. Experimental Details

The measurements were performed at the T9 area of the PS at CERN in September 2015. A primary 24 GeV/c proton beam produced a series of secondary beams from a carbon production target, including kaons, pions, muons and electrons and their antiparticles. We have focused on the positrons in the few GeV energy range. Two Cerenkov detectors were set to discriminate the particle identity (PID). A dipole magnet and a collimator set the momentum byte for the experiment. The incident flight path traversed a scintillator (Scint1) for triggering and a second veto scintillator which defined the beam position on the crystal. The first two Delay Wire Chambers (DWC1 and DWC2) provided transverse spatial hit position measurement ( $\Delta x \approx 200 \mu\text{m}$ ). The incident phase space of each particle trajectory could then be measured ( $\Delta \theta \approx 500 \mu\text{rad}$ ). The charged particles could be swept away with the dipole magnet after the crystal position and their momentum reconstructed from their deflection as measured in the third chamber (DWC3). The radiated photon(s) captured in the photon calorimeter (BGO) could be tagged with PID and the momentum of the radiating particle. Calorimetry of the charged particles was performed in a lead glass calorimeter array. Figure 4 illustrates this

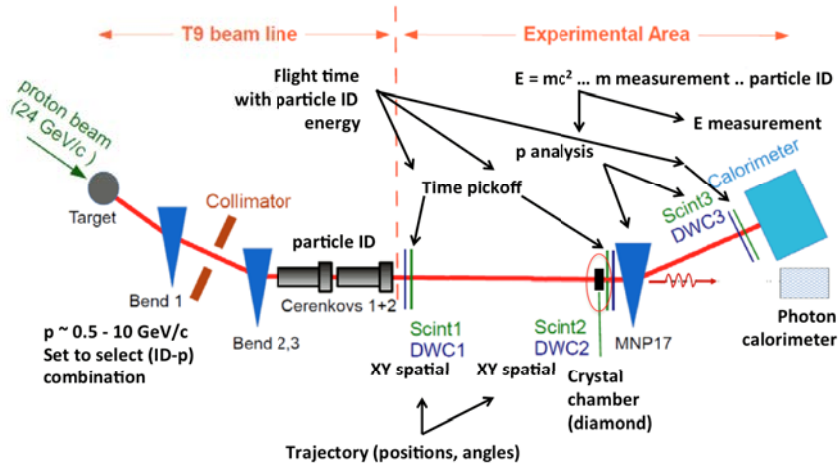


Figure 4: The tagged photon beam-line at the PS-T9 area at CERN (modified from [2]).  
discussion.

## 5. Analysis of Data

### 5.1. Initial validation

The data was available as an event by event stream in a ntuple which could be processed offline using the ROOT C++ analysis framework [12]. Particle tracking, particle identification, incident angle reconstruction, particle deflection, particle energy and momentum measurement, photon energy measurement, photon tagging could all be successfully established and validated. Some of these steps are described below.

### 5.2. Drift-chamber commissioning

Figure 5 below left shows the expected linear correlation between the positron hit position for the x-axis on the first two delay wire chambers, DWC1 and DWC2. The full beam envelope has been filtered in reconstructed incident angle phase space to show only those trajectories closely parallel to the ideal central path. The neighbouring plot shows the difference between the actual hit position on the last delay wire chamber, DWC3, and the projected hit position based on the trajectory reconstructed from DWC1 and DWC2. The third DWC3 could be used to measure the deflection and hence reconstruct the momentum of the beam after the dipole MNP17 in Figure 4. A positron which radiated a photon would have a hit in DWC3 with a greater deflection (lower momentum). Gating on positrons which radiated was used indicating the facility had a tagged photon beam-line.

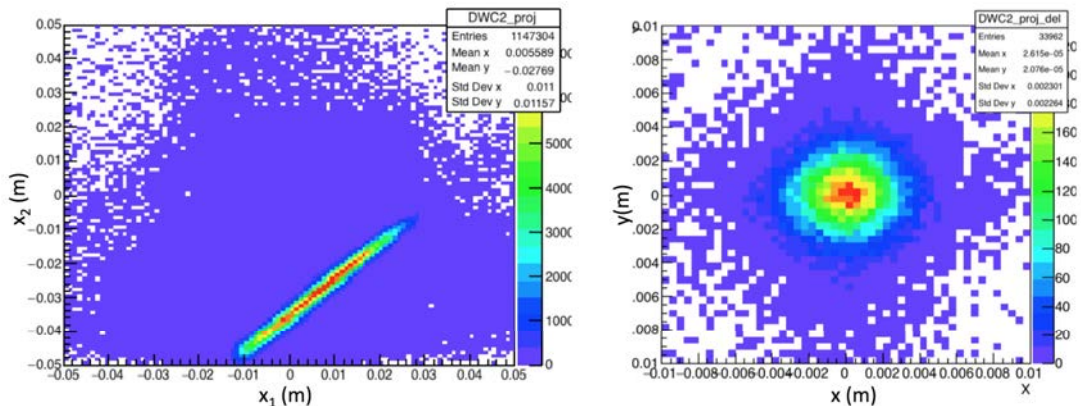


Figure 5: The correlation between x-DWC1 and x-DWC2 (left) and the difference between the actual hit position on DWC3 and the projected hit position based on the trajectory reconstructed from DWC1 and DWC2 (right)

5.3. Event selection and background reduction

The red and black scatter plots in Figure 6 below show the evolution of the beam envelope in DWC1, DWC2 and DWC3 when a elliptic cut is made on the first DWC1. The veto scintillator is next to DWC2, and the operation of this device is clear. The incident angle ( $\theta_x, \theta_y$ ) for each particle could be calculated, and a further cut could be made within this two-dimensional phase space, restricting the divergence within the beam envelope. The final plot in Figure 6 is the photon spectrum in the photon calorimeter for a calibration positron beam energy of 1 GeV. All the curves exhibit a positron peak at the nominal beam energy, as well as a broad photon spectrum with the typical  $1/E$  shape for bremsstrahlung. A peak due to muons passing through the photon calorimeter with the fixed energy loss of minimum ionising particles is also evident at 0.25 GeV. The bremsstrahlung background could be reduced and the muons could be excluded by the filters described above.

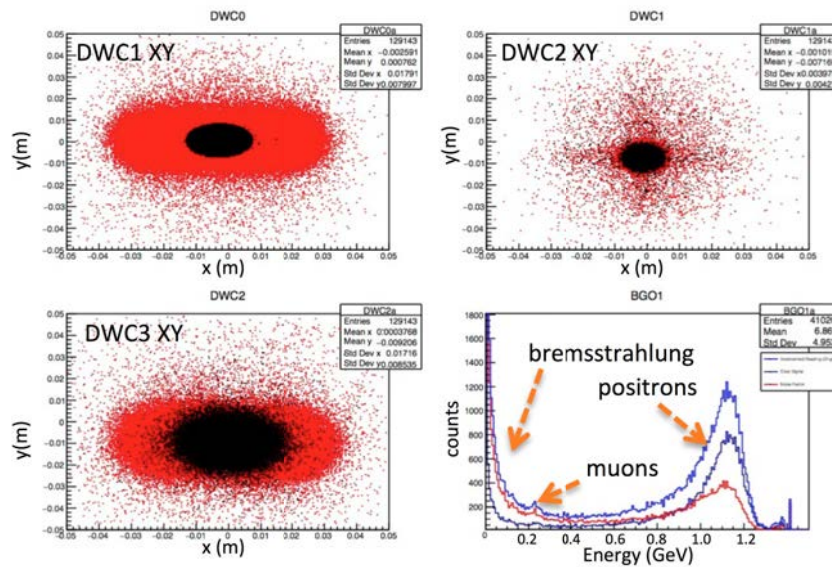


Figure 6: Scatter plots for the three DWCs under the conditions described in the text above. The last plot is the photon spectrum from the photon calorimeter.

5.4. Selection of events aligned to the crystal axis

The critical angle for CR for 6 GeV positrons incident on the 110 axis of diamond is  $\theta_c = 86 \mu\text{rad}$ .

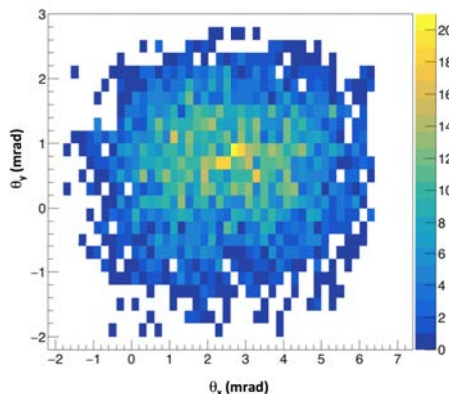


Figure 7: Incident angle phase space.

The two dimensional incident angle phase space plot on the left shows that the useful beam divergence had a range of  $\Delta\theta_x = 3 \text{ mrad}$  and  $\Delta\theta_y = 6 \text{ mrad}$ . The angular resolution is about  $0.3 \text{ mrad}$ . This was larger than anticipated and would smear out evidence of enhanced yield for aligned radiation phenomena. The incident angle space was scanned for enhanced radiation yields based on CR and coherent enhanced BR, in order to fine-align the diamond to the beam axis. Graphical cuts were placed to define the incident angle phase space leading to aligned or non-aligned radiation phenomena. The Figures 8

(filtering events away from axial / planar incidence) and 9 (filtering events close to axial / planar incidence) below are examples of this, where the former yields the expected flat spectrum for BR.

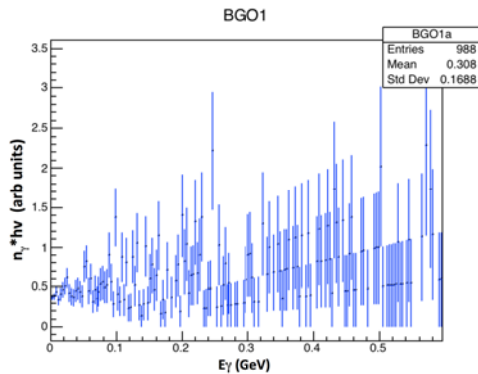


Figure 8: Photon calorimeter selecting for non-aligned incidence events.

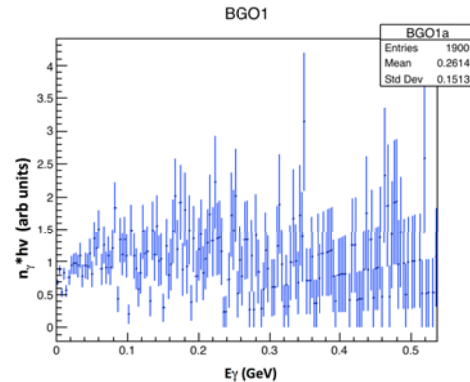


Figure 9: Photon calorimeter selecting for aligned incidence events.

## 6. Conclusion

In the experiment time available it was possible to successfully commission the T9 beam-line of the CERN PS as a tagged photon beam-line. In this set-up, there was large BR background mostly resulting from beam-air interaction upstream of the target. The DWCs unfortunately had a poor resolution, leading to insufficient angular resolution. Suggestive but inconclusive results were obtained (higher radiation yields for aligned incidence). Nonetheless it was sufficiently promising to show that given certain improvements, the T9 beamline could indeed be expected to perform sufficiently well to search for CUR in a future experiment.

## 7. Acknowledgements

The authors thank CERN for the successful operation of the T9 beamline of the CERN PS in the CERN Beamline for Science project.

## References

- [1] Paroli B and Potenza M 2017 *Advances in Physics X* 2-3 978–1004
- [2] 2015 *CERN Beamline for Schools* URL <http://beamline-for-schools.web.cern.ch>
- [3] Tabrizi M, Korol A V, Solov'yov A V and Greiner W 2007 *Physical Review Letters* **98** 164801
- [4] Korol A V, Solov'yov A V and Greiner W 1998 *Journal of Physics G* **24** L45
- [5] Korol A V, Solov'yov A V and Greiner W 1999 *International Journal of Modern Physics* **E8** 49
- [6] Kostyuk, A et al 2009 *J. Phys. G: Nucl. Part. Phys.* **36** 025107
- [7] Kostyuk A 2013 *Phys. Rev. Lett.* **110** 115503
- [8] Brunet F, Germe P *et al.* 1998 *Diamond and Related Materials* **7** 869–873
- [9] Backe H, Krambrich D and *et al.* 2013 *Diamond and Related Materials* **309** 37–44
- [10] Guzmán de la Mata B *et al.* 2007 *Diamond and Related Materials* **16** 809–814
- [11] Krause W, Korol A, Solov'yov A and Greiner W 2002 *Nucl. Instrum. Methods A* **483** 455–460
- [12] Brun R and Rademakers F 1997 *Proceedings AIHENP'96 Workshop, Lausanne, Sep. 1996, Nucl. Inst. & Meth. in Phys. Res. A* **389** 81–86 URL <http://root.cern.ch/>